Influence of Heat Transfer and Material Temperature on Combustion Instabilities in a Swirl Burner

Christian Kraus, Laurent Selle, Thierry Poinsot, Christoph M. Arndt, Henning Bockhorn

Christian Kraus[1]
Institut de Mécanique des Fluides de Toulouse,
UMR CNRS/INP-UPS 5502,
Toulouse 31400, France
e-mail: christian.kraus@imft.fr

Laurent Selle
Institut de Mécanique des Fluides de Toulouse,
UMR CNRS/INP-UPS 5502,
Toulouse 31400, France

Thierry Poinsot
Institut de Mécanique des Fluides de Toulouse,
UMR CNRS/INP-UPS 5502,
Toulouse 31400, France

Christoph M. Arndt
Institute of Combustion Technology,
German Aerospace Center (DLR),
Stuttgart 70569, Germany

Henning Bockhorn
Engler-Bunte-Institute,
Combustion Technology,
Karlsruhe Institute of Technology,
Karlsruhe 76131, Germany

Influence of Heat Transfer and Material Temperature on Combustion Instabilities in a Swirl Burner

The current work focuses on the large eddy simulation (LES) of combustion instability in a laboratory-scale swirl burner. Air and fuel are injected at ambient conditions. Heat conduction from the combustion chamber to the plenums results in a preheating of the air and fuel flows above ambient conditions. The paper compares two computations: In the first computation, the temperature of the injected reactants is 300 K (equivalent to the experiment) and the combustor walls are treated as adiabatic. The frequency of the unstable mode (≈ 635 Hz) deviates significantly from the measured frequency (≈ 750 Hz). In the second computation, the preheating effect observed in the experiment and the heat losses at the combustion chamber walls are taken into account. The frequency (≈ 725 Hz) of the unstable mode agrees well with the experiment. These results illustrate the importance of accounting for heat transfer/losses when applying LES for the prediction of combustion instabilities. Uncertainties caused by unsuitable modeling strategies when using computational fluid dynamics for the prediction of combustion instabilities can lead to an improper design of passive control methods (such as Helmholtz resonators) as these are often only effective in a limited frequency range. [DOI: 10.1115/1.4035143]

1 Introduction

The occurrence and the avoidance of combustion instabilities are still major challenges in the design and operation of modern combustors [1,2]. Large eddy simulation (LES) has proven to be an adequate tool to investigate combustion instabilities and the underlying mechanisms that cause the coupling between pressure and heat release rate oscillations [3–6]. As computational resources are more and more available, LES is nowadays also successfully applied to study combustion instabilities in real combustors with complex geometries [7]. In addition, LES can be combined with tools with significantly lower computational cost. Helmholtz solvers provide the possibility to study unstable modes in the frequency domain [3,8].

However, the complex interaction between flame and acoustics is still not fully understood. For example, recent studies show the existence of flame-intrinsic instabilities [9–11]. Their impact on and contribution to the development of unstable modes in combustors, especially in real engines with complex geometries, is difficult to assess. In addition, both acoustics and heat release rate oscillations can be influenced by additional nonstationary physical mechanisms. Heat transfer between solid materials and fluids and heat transfer by heat conduction inside the solid material are important examples that can affect combustor dynamics. Temperature variations caused by heat transfer influence both the acoustic behavior of the combustor and the flame response characteristics: they lead to changes in sound speed and can affect the velocity field and mixing processes and therefore alter flame speed and flame shape. In this context, two important cases of heat transfer are:

- the heat transfer from the hot combustion chamber to the combustor parts located upstream of the combustion chamber (swirler/injector, plenum)
- the heat losses at the combustor walls, particularly at the combustion chamber walls

In the direct numerical simulation analysis of Duchaine et al. in Ref. [12], it is shown that the flame response of a confined laminar premixed flame to acoustic perturbation is significantly influenced by the wall temperature of the inlet duct into the combustion chamber and the flame speed. An increase in the duct wall temperature results in an acceleration of the fresh mixture and an increase of the local flame speed. As a consequence, the delay of the flame transfer function (FTF) decreases. Lohrmann and Buechner [13] also observed a diminution of the delay of the flame response at higher preheat temperatures and a strong impact of the preheat temperature on the amplitude response of the flame. They explain the smaller delay with an increase of the turbulent flame speed at higher preheat temperatures, which moves the main reaction zone closer to the nozzle outlet. Kaess et al. [14] observed in their simulation of a laminar premix flame that the flame position changes when switching from adiabatic to isothermal combustion chamber walls. The FTF of the flame in the case with isothermal walls showed a significantly better agreement with the experimentally obtained FTF. Mejia et al. [15] showed in their experiment that the combustion instability observed in a laminar premixed flame can be triggered by activation of the cooling system of the burner rim. They concluded that the burner rim temperature alters the flame root dynamics, which affects the FTF. Low temperatures of the burner rim increased the flame root dynamics in the frequency range of the instability and thus lead to a stronger flame response. Hong et al. [16] observed that the dynamic instability characteristics of an unstable mode in a turbulent premixed backward-facing step combustor are influenced by the heat transfer characteristics near the flame-anchoring region. They carried out experiments with two different materials for the flame holder (stainless steel and ceramics) and found out that using the material with the lower thermal conductivity (ceramic) delayed or prevented the onset of the instability after combustor ignition. They concluded that this behavior is caused by variations of the flame speed which are induced by the different thermal conductivities of the used materials. The effect of varying the preheat temperature on the flame response of spray flame subjected to fuel flow rate modulations were investigated by Yi et al. in Ref. [17]. With increasing preheat temperature, the flame became more responsive to fuel flow rate modulations, which was mostly caused

[1]Corresponding author.

by a decrease of the evaporation and chemical time scale with higher temperatures. In the liquid fuel combustor investigated by Hassa et al. [18], the resonance frequency of the system depended only on the preheat temperature, whereas the amplitude response of the system was strongly influenced by the burner geometry.

Modeling heat transfer in a numerical simulation can increase the computational effort. However, it can be of great importance for the adequate prediction of combustion instabilities: Shahi et al. [19] observed a significant influence of the wall boundary conditions on the frequency of the unstable mode in their simulation of the Limousine combustor.

In this paper, we investigate the combustion instability observed in a laboratory scale burner, which is operated at Karlsruhe Institute of Technology (KIT), Karlsruhe, Germany and DLR, Stuttgart, Germany. The combustor can be operated as single burner and multiple burner and has already been studied in both configurations [20,21]. No preheating is applied to the reactants, which leads to inlet temperatures of about $T = 300\,\mathrm{K}$. At the investigated operating point, the combustion instability occurs after a certain warm-up phase. During the warm-up, the temperatures of the air flows inside the plenum rise to values above ambient conditions. The presented results show that in order to obtain an adequate prediction of the frequency of the unstable mode, it is of great importance to account for the heat transfer from the combustion chamber to the plenum.

After the introduction, the combustor and the experimental setup are explained, followed by the description of the numerical setup for the performed calculations. Subsequently, the results and the outcomes of the calculations are discussed in detail.

2 Experimental Setup

The combustor is operated under atmospheric conditions, using gaseous fuel. Experiments are performed with natural gas (>90% CH_4, KIT) and pure methane (DLR). The differences in the fuel composition do not show a significant effect on the combustor dynamics; differences in frequency of the unstable modes are around 1.5%. The flame is swirl-stabilized using a double-concentric swirl nozzle. The swirlers employ separate air supplies, which allow controlling the air flows through each swirler independently (Fig. 1). The fuel plenum is located inside the inner tube of the inner plenum. The fuel flows through the nozzle (between the outer and the inner swirler) and exits the nozzle through 60 circumferentially distributed holes with a diameter of 0.5 mm. It is then injected into the air flow of the inner swirler, which leads to flames of partially premixed character.

For optical access, the combustion chamber is equipped with quartz glass windows. Perforated plates are installed in the plenums to homogenize the air flows in the swirler plenums. Microphone probes measure pressure oscillations in the combustion chamber and the plenums. The air temperatures in the plenums are monitored with thermocouples.

The three-component velocity field in the combustion chamber was measured at DLR Stuttgart using a stereoscopic particle image velocimetry (S-PIV). The measurement system (LaVision Flow Master) consisted of a frequency-doubled, dual head Nd:YAG laser (New Wave Solo 120) and two CCD cameras (LaVision Imager Intense, 1376×1040 pixels), which were operated in dual-frame mode. The laser energy was 120 mJ/pulse at 532 nm, and the pulse repetition rate was 5 Hz, and the pulse separation time between the double pulses was 8 μs. The laser was formed into a light sheet with a thickness of 1 mm using a two-stage Galilean telescope, spanning the complete height of the combustion chamber, and directed through the symmetry plane of the combustion chamber. Mie scattering from titanium dioxide particles (nominal diameter 1 μm) was imaged onto the cameras using wide-angle lenses ($f = 16\,\mathrm{mm}$, $f/2$), equipped with a band-pass filter (532 nm $\pm$ 5 nm) in order to suppress background luminosity. To protect the cameras from thermal radiation, an IR filter was placed between the combustion chamber and the cameras.

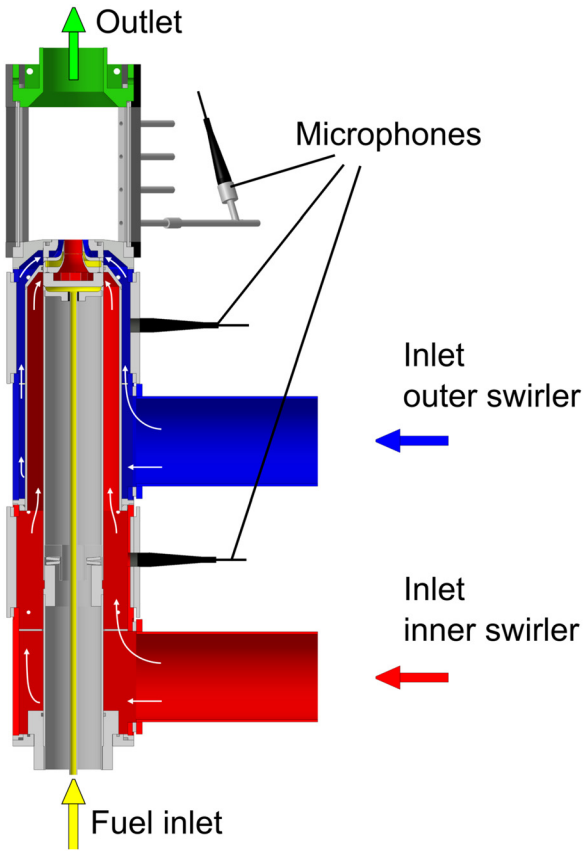

Fig. 1 Swirl combustor with two air inlets and locations of microphone probes

Scheimpflug adapters were used to align the focal plane of the cameras to the measurement plane. Both cameras had a viewing angle relative to the measurement plane of 20 deg, and the distance between the cameras and the measurement plane was 200 mm. The field of view covered the area $-39\,\mathrm{mm} < r < 39\,\mathrm{mm}$ and $0.5\,\mathrm{mm} < h < 105\,\mathrm{mm}$. A total of 1200 particle pair images were recorded, and the vector fields were calculated using commercial PIV software (LaVision DaVis 8.0). A multiscale cross-correlation algorithm was used, resulting in a final interrogation window size of 16×16 pixels with 50% overlap, corresponding to a vector resolution of 1.5 mm and a vector spacing of 0.75 mm. The relaxation time of the particles was $t_{\mathrm{relax}} = 5 \times 10^{-6}$ s, the maximum local velocity differences were $\Delta v = 70\,\mathrm{m/s}$ and occurred over a length scale of $\Delta l = 10\,\mathrm{mm}$. The resulting Stokes number is $t_{\mathrm{relax}}\,\Delta x/l < 0.04$, and thus velocity errors due to particle slip are considered negligible. With the 0.1 pixel uncertainty of the PIV algorithm, the maximum random in-plane uncertainty is $< 1.2\,\mathrm{m/s}$. With a camera angle relative to the imaging plane of 20 deg, the uncertainty of the out-of-plane velocity is about three times higher as the uncertainty of the in-plane velocity [22].

3 Numerical Setup

3.1 Flow Solver. The numerical simulations discussed in this paper were performed with the AVBP code developed at CERFACS and IFPEN. It solves the compressible Navier–Stokes equations on unstructured meshes. The spatial discretization in AVBP is based on the finite volume method with a cell-vertex approach. The applied numerical scheme is the Lax–Wendroff scheme, which is of second order in time and space and the maximum CFL number is set to 0.9.

The Subgrid stresses are modeled with the classical Smagorinsky model ($C_s = 0.18$). The flame/turbulence interactions are modeled with the dynamic thickened flame model [23,24]. This

combustion model has already been successfully applied in numerous studies, as for example in Refs. [25–27]. Chemistry is modeled using a two-step mechanism for methane/air flames (BFER, [28]) with two reactions and six species (CH_4, O_2, CO_2, CO, H_2O, and N_2). The first reaction is irreversible and controls the oxidation of CH_4 while the second reaction is reversible and leads to equilibrium between CO and CO_2.

3.2 Mesh and Boundary Conditions. The mesh used for the computations is a fully tetrahedral mesh with 4.6×10^6 cells and was generated with the commercial software CENTAUR. Plenum and combustion chamber are fully modeled (Fig. 2). The mesh is refined in the outlet region, as well as in the mixing zone of fuel and air and in the region where the flame is located.

Boundary conditions are treated by the Navier–Stokes characteristic boundary conditions (NSCBC) method [29]. The inlets are modeled to be nonreflective; therefore outgoing acoustic waves can leave the domain. The outlet of the burner in the experimental setup exits into to the ambient atmosphere and therefore corresponds to an acoustically open end. One possibility to model such an outlet is to mesh a portion of the surrounding atmosphere [4]. In the present work, a different approach is taken. To model the acoustic impedance, the relaxation coefficient (for further details, see Ref. [30]) of the outlet boundary condition was adjusted to match the impedance of the acoustically open end, which is calculated according to the model of Levine and Schwinger [31]. The model of Levine and Schwinger provides an adequate modeling of the impedance of an open pipe even in the presence of mean flow [32]. Figure 3 compares the impedance of the applied boundary condition with the impedance given by the model of Levine and Schwinger. The curves of both the modulus of the reflection coefficient and the phase are similar in the relevant frequency range (0–2000 Hz). The current approach was verified on a simple test case (not discussed here) and allows for performing the computations with adequate impedance of the outlet without meshing the surrounding atmosphere or increasing the length of the outlet tube. The perforated plates installed in the plenums of the combustor feature around 190 and 90 holes, respectively, with a diameter of 2 mm. This results in porosity of around 10% for both perforated plates. A proper resolution of the flow inside the holes is computationally very costly. Therefore, the acoustic behavior of the perforated plates is modeled with a modified Howe model which is discussed in detail in Refs. [33,34]. Since the Strouhal numbers of the discussed unstable modes are relatively small ($St < 0.5$), the application of the Howe model is still justified, although the influence of interaction effect of the orifices (which is not accounted for in the Howe model) can significantly alter the acoustic impedances of perforated plates with porosities around 10% [35].

The Reynolds numbers of the flow in the plenums are $Re < 2500$; therefore, no-slip boundary conditions are imposed on the walls in the plenums. In the swirlers, as well as in the combustion chamber, Law-of-the-wall models [36] are used to calculate the velocity profiles at the walls, except for the outlet region of the combustion chamber. The choice to refine the mesh instead of using wall models was made in order to reproduce well the flow conditions in the outlet tube. It was observed that the mesh resolution in the outlet region has a strong impact on the acoustic behavior of the combustion chamber. In addition, wall models are not suited to compute the velocities in zones where flow separation takes place, as in the section constriction of the outlet tube. However, the mesh in the outlet region does not fully resolve the wall boundary layer ($y^+ \approx 2$-5). This was considered to be the best compromise between accuracy and computational cost.

In case of a nonadiabatic and nonisothermal wall, the heat flux is calculated according to Fourier's law using the (assumed

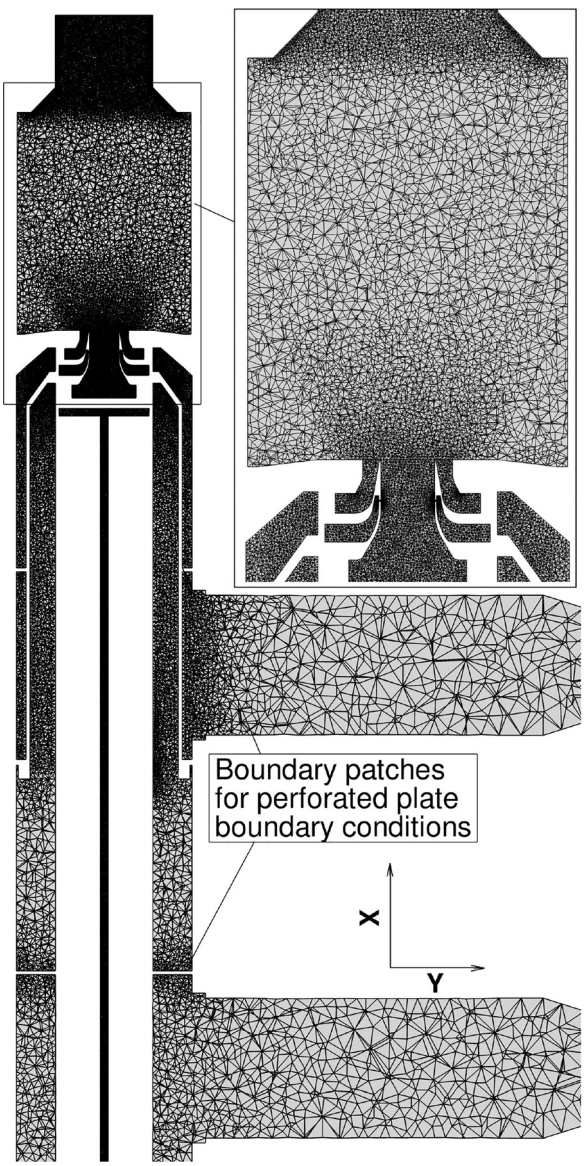

Fig. 2 Cut of the mesh in the middle plane. The domain is separated at the boundary patches for the perforated plates. The corresponding patches are coupled with the modified Howe model.

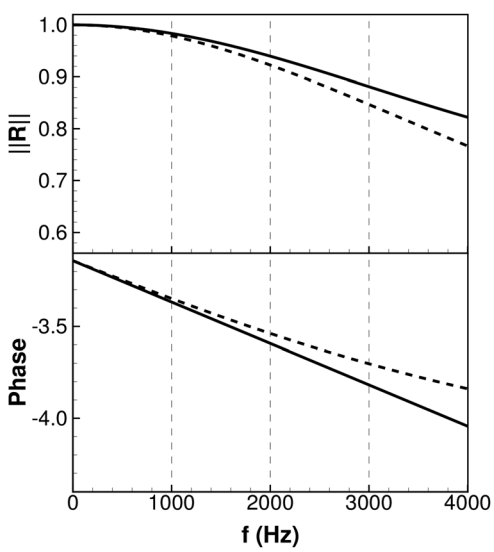

Fig. 3 Modulus and phase of the reflection coefficient *R* of the combustion chamber outlet: —— Levine and Schwinger [31], – – – – AVBP with adequate relaxation coefficient

constant) thermal conductivity of the material and the temperature gradient between a defined reference temperature and the local wall temperature.

4 Operating Point and LES Cases

The investigated operating point has a thermal power of $P_{th} = 30\,\text{kW}$ with a global equivalence ratio of $\phi = 0.85$. The air split ratio $L = \dot{m}_{OTS}/\dot{m}_{IS}$ (OTS = outer swirler, IS = inner swirler) of the investigated operating point is set to $L = 1.6$, which results in approximately equal pressure drops over both swirlers. The specifics of the LES cases are summarized in Table 1.

Case 1 does not take into account any heat losses or heat transfer inside the combustor. The inlet temperatures of $T = 300\,\text{K}$ correspond to the temperature in the air supply in the experiment and all walls are considered as adiabatic.

Case 2 accounts for both the heat losses of the combustion chamber to the ambient atmosphere and for the heat transfer from the hot combustion chamber frame to the plenum. However, instead of modeling heat conduction inside the solid material and/or heat transfer from the hot plenum walls to the flow, the inlet temperatures are increased above ambient conditions. This represents of course a simplification compared to the experiment, as the temperature distribution inside the plenum is most likely not homogenous, and may have an influence on the results. Nevertheless, as the exact temperature distribution is not known, it was decided to match the air flow temperature in the LES to the air temperatures measured in the experiment instead of making assumptions for the plenum wall temperatures and heat conductivities. Therefore, the temperatures at the inlets of $T = 450\,\text{K}$ for the outer plenum and $T = 350\,\text{K}$ for the inner plenum correspond to the temperatures measured with the installed thermocouples. The inlet temperature of the fuel plenum was set to the inlet temperature of the inner plenum.

The reference temperatures (T_{ref}) for the calculation of the heat losses at the combustion chamber walls are shown in Fig. 4. In the calculation of the heat fluxes, the thermal conductivity of the corresponding material (quartz glasses or stainless steel) is used. A constant temperature (T_{iso}) is imposed at the dump plane of the combustion chamber. The reference temperatures at the side walls of the combustion chamber are assessed from measurements with thermocouples. The remaining temperatures are estimated based on the annealing colors of the combustion chamber parts observed during combustor operation (not shown here).

5 Results and Discussion

5.1 Comparison of PIV and LES. The mean flow fields in both LES cases correspond to an averaging time of about $t = 0.06\,\text{s}$. Figure 5 shows the axial locations where the profiles are extracted. Figure 6 compares the profiles of the mean velocities of the PIV and the LESs of cases 1 and 2. The velocity field is typical for a swirled flow, with negative axial velocities on the burner axis and a recirculation zone. A good agreement between experiment and simulation is observed for the absolute mean axial velocities. However, the mean radial and the tangential velocities of both LESs exceed the measured values, in particular near the nozzle outlet.

The root mean squares (RMSs) of the velocity fluctuations are higher in the LES compared to the experiments (Fig. 7). However, the global shapes of the profiles are similar, except for the RMS of the radial velocity in case 1, which significantly exceeds the RMSs of the radial velocity observed in case 2 and the experiment. This is caused by a transverse acoustic mode in the combustion chamber,

Table 1 Specifics of the LES cases (CC = combustion chamber, OTS = outer swirler, IS = inner swirler)

Case	Walls CC	T at inlet OTS	T at inlet IS
1	Adiabatic	300 K	300 K
2	With heat losses	450 K	350 K

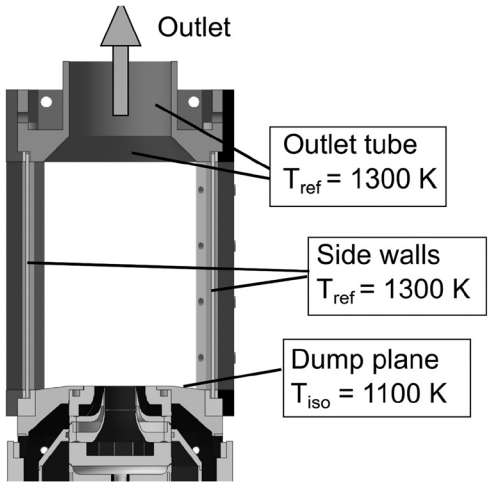

Fig. 4 Reference temperatures (T_{ref}) and constant temperature (T_{iso}) for the modeling of the heat losses at the combustion chamber walls

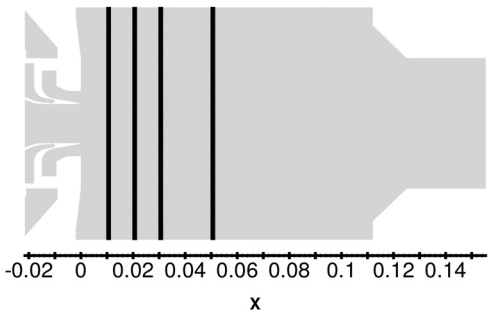

Fig. 5 Axial locations of the extracted profiles

which is only observed in the LES of case 1 and results in augmented velocity oscillations in the radial direction on the burner axis.

To summarize, it can be stated that the PIV measurements and the LESs agree fairly well in terms of the overall trend of the profiles. However, some general observations are made in the comparison of the results of the PIV and the LES cases, which require further discussion: (1) In both LESs, the mean velocities and RMSs are increased compared to the experiment. (2) The LES of case 2 shows higher mean velocities and RMSs than the LES of case 1, which results in larger deviations from the experiment compared to case 1.

The deviation between experimental and numerical results can have several reasons. It is possible that the mesh resolution is not sufficient near the nozzle outlet. Furthermore, in both LES cases, the imposed thermal boundary conditions may lead to temperature fields that do not exactly reproduce the conditions in the experiment. This can be expected for case 1, since the walls in the experiment are clearly not adiabatic. However, the modeling of heat transfer in the LES of case 2 does not lead to smaller discrepancies between experiment and simulation, but results in larger deviations from the experiment. The reason for this is that the mean temperatures in the LES of case 2 exceed the ones in case 1 except for the near wall region (Fig. 8); this is consequently also the case for the mean velocities. A significant decrease of the temperature due to the heat losses in case 2 is only observed close to the walls. The thermal boundary conditions in the combustion chamber (as these are mostly based on estimated values), in combination with the increased inlet temperatures in case 2, may lead to temperature distributions and/or main reaction zones which differ from the experiment. Temperatures are possibly be too high near the nozzle outlet; this leads in turn to higher mean velocities than in the experiment and/or results in differences in the locations of the main reaction zones. Since the temperature gradients

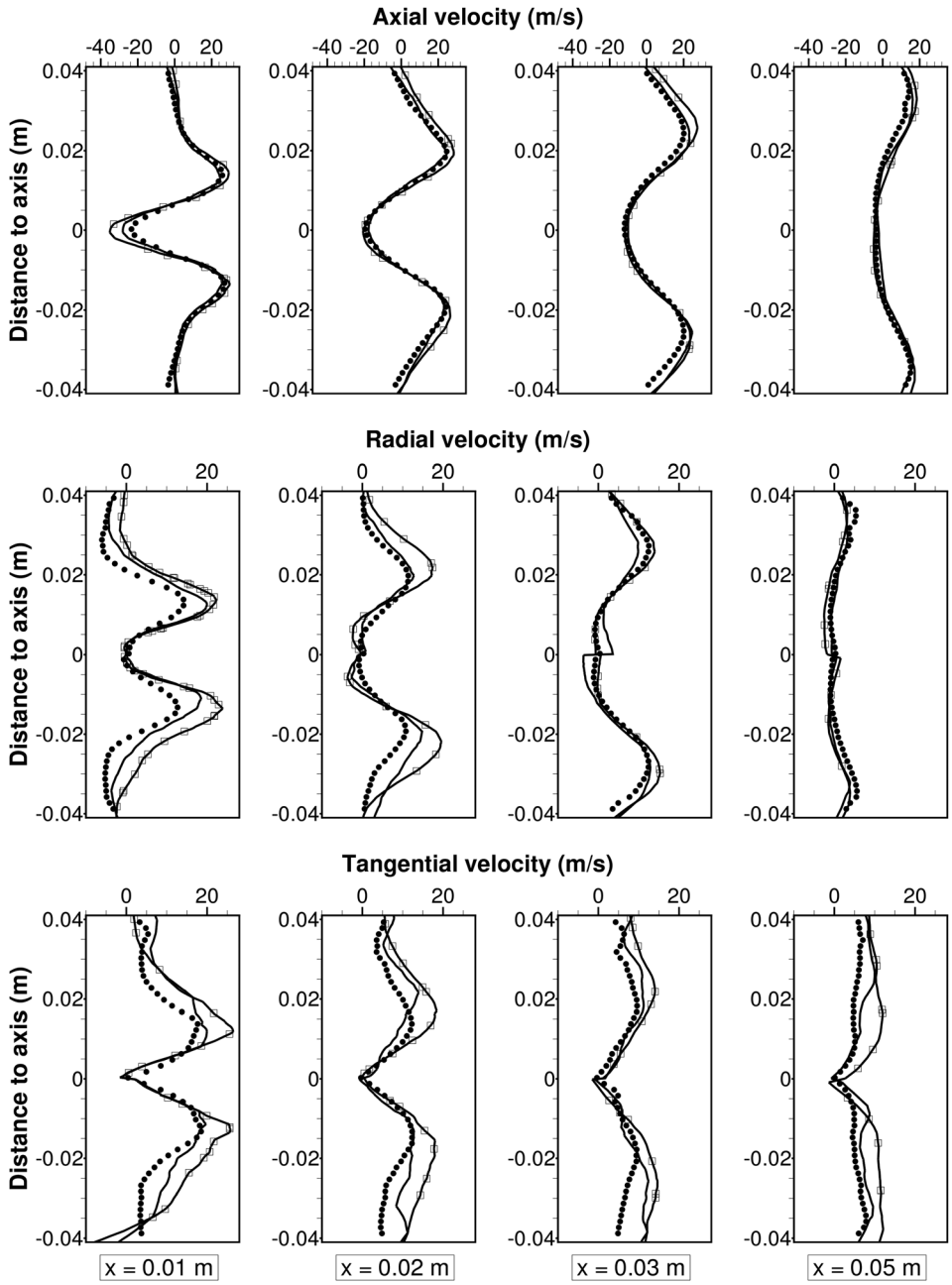

Fig. 6 Time-averaged mean velocities in the experiment (•) and the LESs of case 1 (——) and case 2 (— □ —); x = distance to nozzle outlet

are large in this region (Fig. 8), slight differences in the temperature profiles between experiment and simulation can lead to significant differences in the velocity profiles.

It also has to be considered that Favre averages computed by compressible LES can deviate from averages measured with PIV, as these are usually considered as Reynolds averages [37]. Especially in zones with high temperature fluctuations, Favre averages can deviate from Reynolds averages [38]. In the present simulations, the RMSs of the temperature fluctuations are in fact very high near the nozzle outlet (Fig. 8, $x = 0.01$ m). Further downstream at $x = 0.03$ m, where the values of T'_{RMS} are decreased, the agreement between the LESs and the PIV is also better, which indicates that the mentioned discrepancies between Favre and PIV averages contribute to the differences between experiment and simulation. A similar observation was made in Ref. [4].

The overall RMSs of the velocity fluctuations in the LESs are most probably increased due to the increased amplitudes of the unstable modes compared to the experiment. The unstable mode in case 2 features significantly higher amplitude than in case 1, which explains why the differences in RMSs in case 2 are higher compared to experiment. This is further discussed in Sec. 5.2.

5.2 Unstable Mode and Flame Characteristics. Figure 9 compares the spectra from the experiment and the LES cases. The frequency of the unstable mode in the experiment is in the range of $f = 750$ Hz. The frequency of the dominant mode in case 1 is about $f = 635$ Hz and deviates significantly from the experiment, whereas the frequency of the dominant mode in case 2 ($f = 725$ Hz) is much closer to the experimental value. In both computations, the pressure amplitudes in the plenum and the combustion chamber are significantly higher than in the experiment. Regarding the amplitude of the mode, case 1 is closer to the experiment than case 2. There are many possible reasons for the increased amplitudes in the LESs. However, one important reason is that walls in real combustors are, in contrary to walls in numerical simulations, never perfectly reflecting and absorb a certain

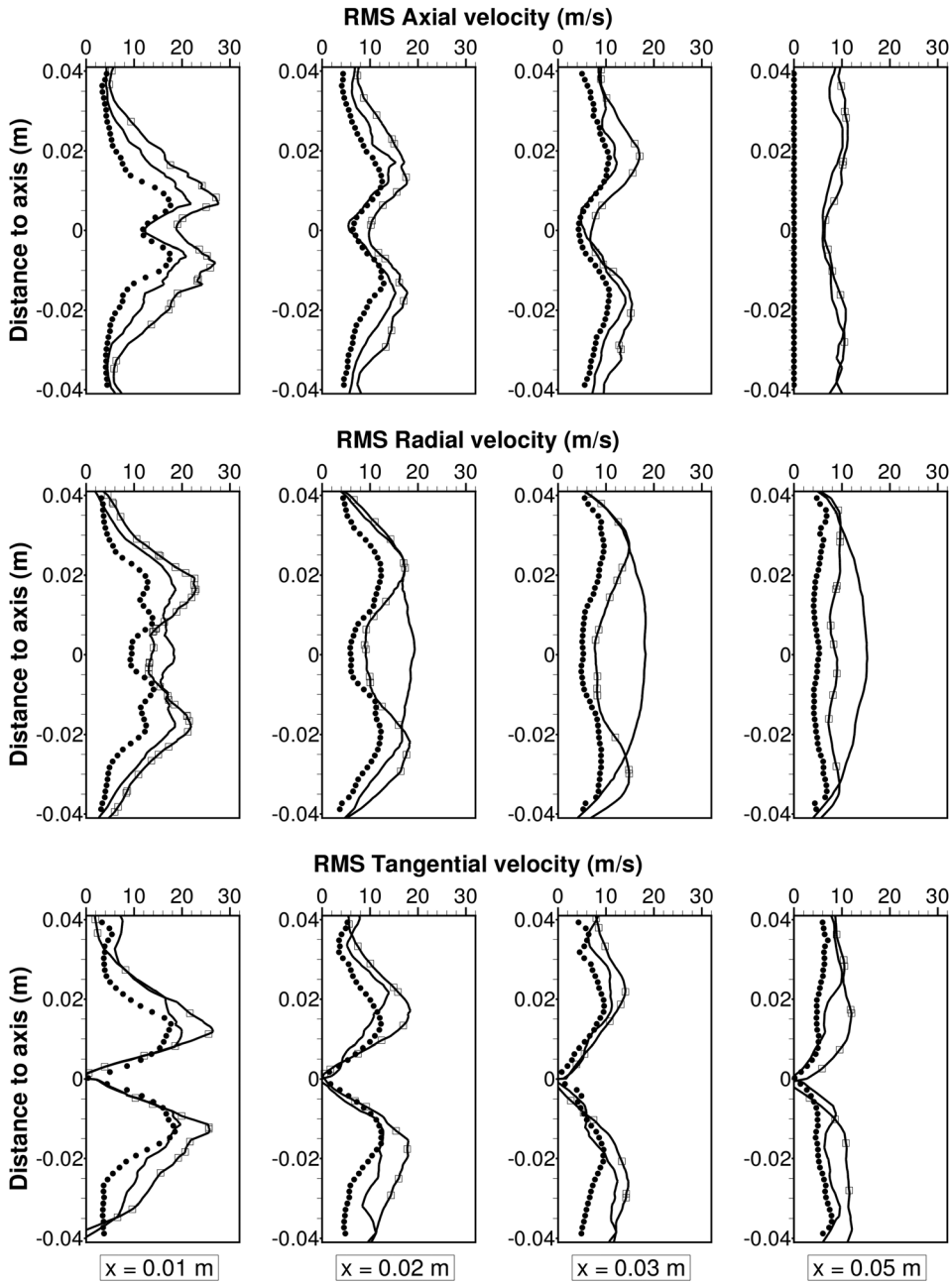

Fig. 7 RMS of velocity fluctuations in the experiment (•) and the LESs of case 1 (——) and case 2 (— □ —); x = distance to nozzle outlet

amount of acoustic energy. As depicted in Fig. 10, the time signal of the pressure probe in case 1 shows the oscillation at $f = 635$ Hz and also the transverse mode at around $f = 5000$ Hz in the combustion chamber that causes the increased fluctuations of the radial velocity on the axis. In the signal of the integral heat release rate, only the mode at $f = 635$ Hz is observed. The time signals of the pressure probe and the integral heat release rate in case 2 mainly show the mode at $f = 725$ Hz. In both cases, pressure and the heat release oscillations are in phase; therefore, as expected, the Rayleigh Criterion [39] is satisfied in both LESs.

In order to verify if in fact the frequency of the instability changes due to the increased inlet temperatures and is not caused by the excitation of a different acoustic mode, the power spectral density of each mode was calculated at each node on extracted 2D cuts of the flow fields in the middle plane of the combustor in order to investigate the mode structure in each case. Figure 11 compares the amplitude and the phase of the unstable modes for both cases. The mode structure in case 1 is similar to the mode structure in case 2. The unstable mode is a coupled longitudinal mode of the combustion chamber and the outer plenum whose structure resembles a 3/4-quarter wave mode. The curves of the amplitude and phase show that in both LES cases, the same mode is excited.

The mean temperature in the combustion chamber is nearly equal in both cases ($T \approx 2000$ K). The increased air temperature in the plenum and the swirler in case 2 have two major consequences that can affect the mode frequency: (1) The sound speed is increased due to the elevated temperatures in the plenum and (2) the flame transfer function may be changed compared to case 2. Since a flame generally shows only minor influence on the frequency of an instability (see, e.g., see Ref. [40] or Ref. [18]), the results indicate that the mode frequency changes between cases 1 and 2 due to the differences in sound speed in the plenum.

The fact that the mode amplitude is augmented in case 2 suggests that the FTF of the flame is also affected by the increased inlet temperatures, as the flame response can vary strongly with frequency [41,42]. Changes in the FTF are often induced by

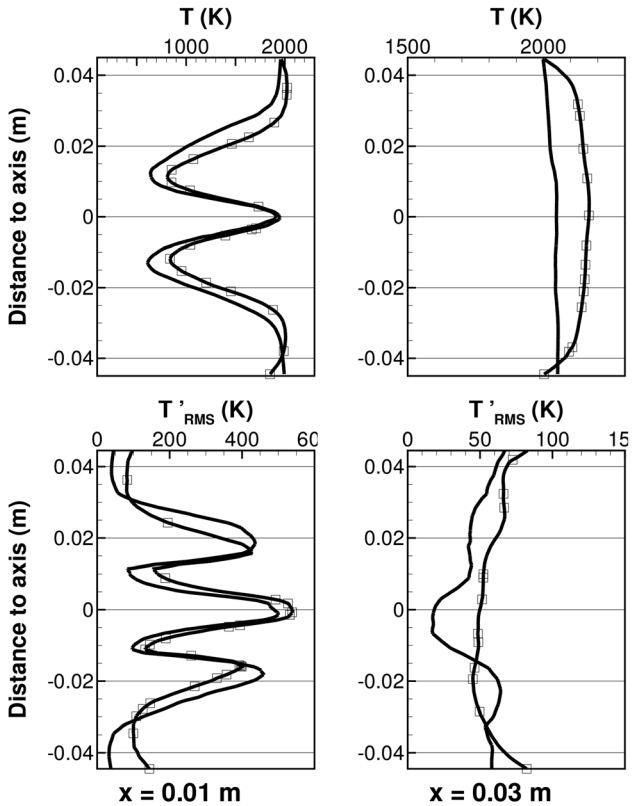

Fig. 8 Temperature profiles in the LESs of case 1 (——) and case 2 (— □ —); x = distance to nozzle outlet

alterations of the flame shape or flame length [43]. Figure 12 shows the mean heat release rates in both LES cases. The flame in case 2 is shorter and more compact. This is most probably caused by the higher inlet temperatures in case 2, which result in increased flame speeds/reaction rates that may in fact affect the flame response. The FTFs of the flames in cases 1 and 2 have not been evaluated, but a comparison of the time-averaged Rayleigh source term in cases 1 and 2 in Table 2 reveals that its value is about 76% higher in case 2, which could explain the increased pressure amplitude in case 2. It has to be considered that the calculated Rayleigh source term represents all modes present in the combustion chamber; in particular also the transverse mode of case 1, whose contribution to the Rayleigh source term cannot be assessed with our current database. The results also present some uncertainties, which illustrate the complexity of defining adequate thermal boundary conditions when performing simulations with heat transfer/losses:

- It is difficult to determine whether the flame shape and the flame position in the experiment are well reproduced in the LES of case 2, since discrepancies in the velocity fields of the PIV and the LES of case 2 are observed, as discussed in Sec. 5.1. Images of the OH* chemiluminescence were taken, but the OH*-intensity distribution can deviate from the heat release distribution in turbulent partially premixed flames [44]. However, to the first order, the response of such a flame is related to its length and position (e.g., see Refs. [13,41]). Consequently, the fact that the instability frequency is well predicted provides an indirect validation of the computed flame shape and position: the frequency of the unstable mode is mainly imposed by the geometry and the sound speed field; with an incorrect delay in the LES, no instability would be observed at this frequency.
- The fact that the mean temperatures in both LES cases are similar raises the question if the imposed thermal boundary conditions in case 2 are suited to model the heat losses in the real combustor, as one would expect a significant decrease in temperature inside the combustion chamber when using non-adiabatic boundary conditions. This can be partially explained by the difference in the average integral heat release rate $\overline{\dot{Q}}$, which almost coincides with the thermal power of $P_{\mathrm{th}} = 30\,\mathrm{kW}$ for case 2 ($\overline{\dot{Q}} - P_{\mathrm{th}} = -5\,\mathrm{W}$), whereas combustion is less complete in case 1 and the average integral heat release rate is about 280 W smaller than the thermal power ($\overline{\dot{Q}} - P_{\mathrm{th}} = -280\,\mathrm{W}$), which corresponds to a temperature difference in the combustion chamber of $\Delta T = 20\,\mathrm{K}$. However, the applied thermal boundary conditions are mainly based on estimations; therefore, the heat losses may be in fact underestimated in case 2.

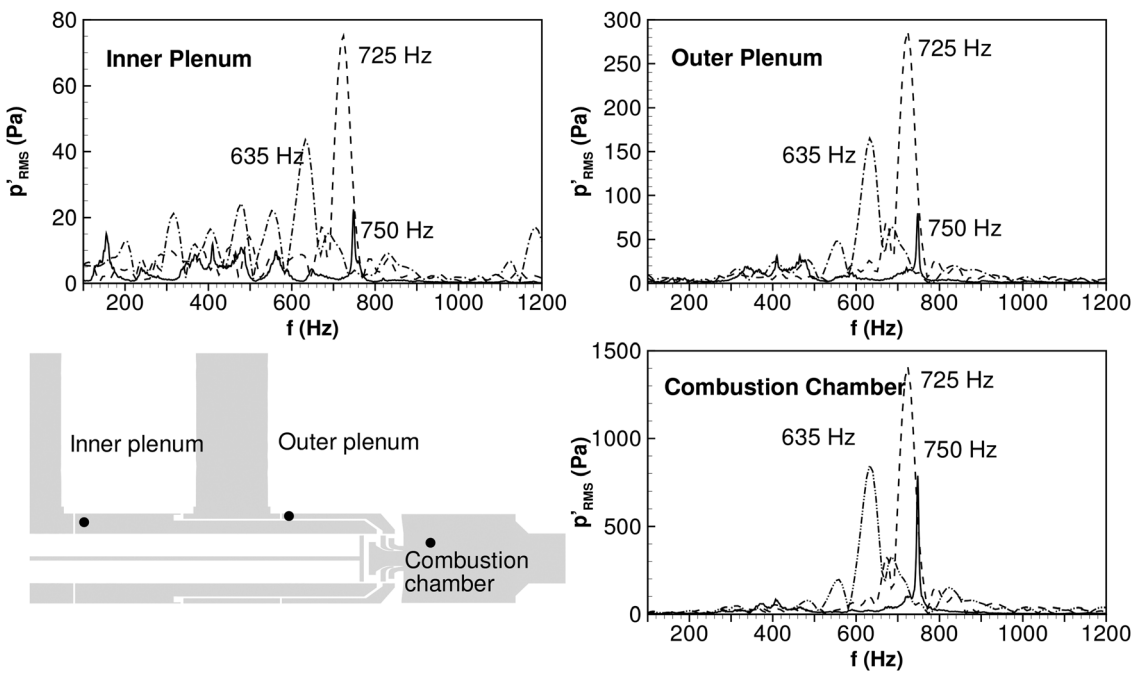

Fig. 9 Pressure spectra in the combustion chamber and the plenums in the experiment (——) and the LESs of case 1 (–. –. –) and case 2 (– – – –)

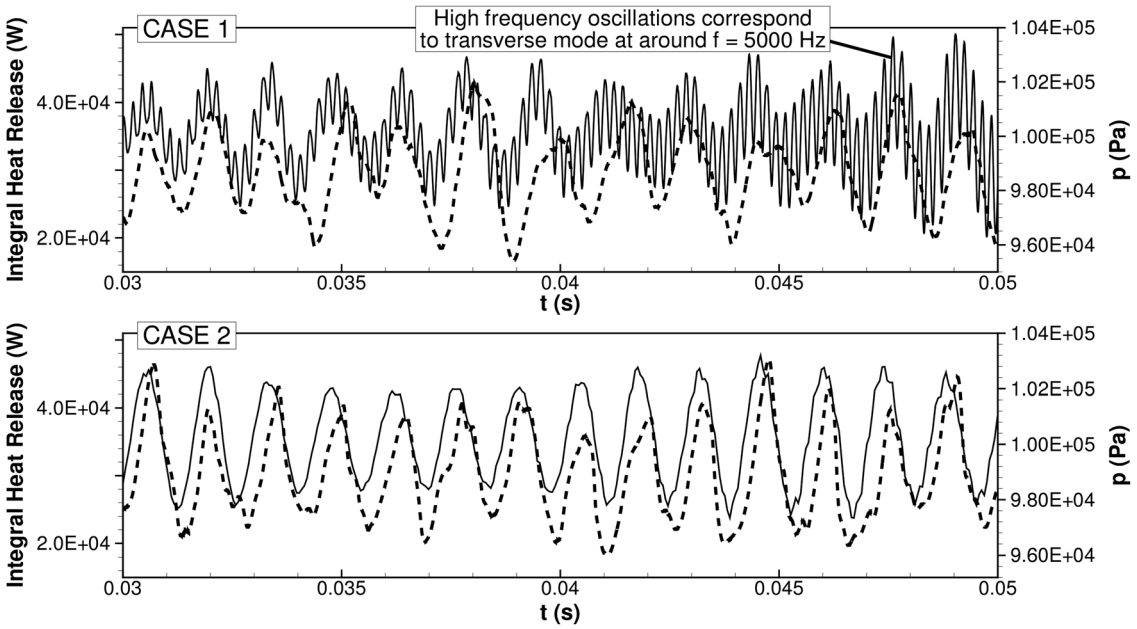

Fig. 10 Time signal of pressure at the probe in the combustion chamber (——) and the integral heat release rate (– – – –)

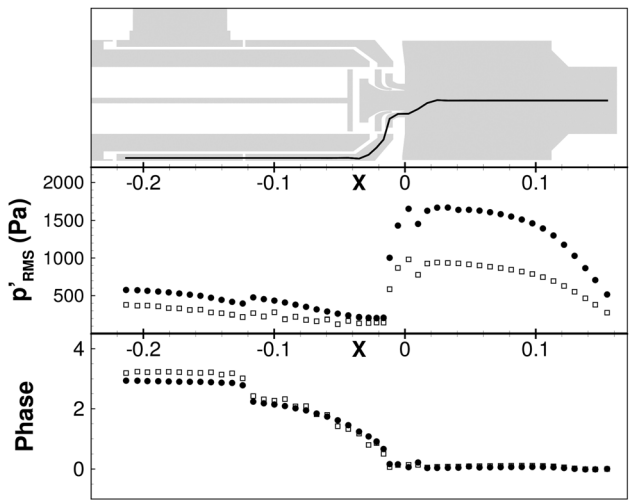

Fig. 11 Moduli and phases of the unstable modes in the LES of case 1 ($f = 635$ Hz, □) and the LES of case 2 ($f = 725$ Hz, •). Modulus and phase were extracted along the shown path in the outer plenum and the combustion chamber.

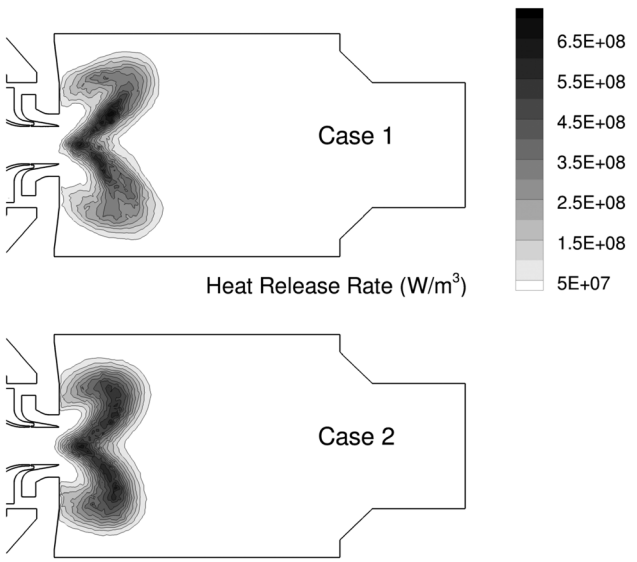

Fig. 12 Average heat release rates in the LESs of cases 1 and 2 (2D cut in the middle of the combustion chamber)

Nonetheless, the discussed uncertainties do not change the main finding of the performed investigations: the influence of the temperature in the plenum on the frequency of instability is very significant due to the changes in the sound speed field. In order to obtain an instability frequency that is similar to the experiment, the heat transfer from the combustion chamber to the plenum has to be considered.

6 Conclusion

In the present work, combustion instability in a swirl burner is analyzed using two LESs with different boundary conditions. In the first case, heat transfer by heat conduction is completely neglected and all walls are treated as adiabatic. In the second case, heat losses at the combustion chamber walls as well as preheating of the air by heat conduction from the combustion chamber to the plenum are accounted for. The average velocities computed by the LESs are compared to PIV measurements. Both cases agree fairly well with the experiment; possible explanations for the observed discrepancies between the results of the LESs and PIV are discussed. The velocities computed in the adiabatic case are in better agreement with the experimental results, but the frequency of the instability deviates significantly from the experiment, whereas the frequency in the LES with modeled heat losses/transfer is quite close to the experimental value. The analysis of the mode structure shows that the mode is similar in both LES cases and represents a coupled mode of combustion chamber and outer plenum. Two possible explanations for the difference in mode frequency between the LES cases are discussed: (1) changes of the sound speed field due to the influence of the modeled heat transfer

Table 2 Time-averaged Rayleigh source term in cases 1 and 2

Rayleigh source term (W)	Case 1	Case 2
$\frac{\gamma-1}{\gamma\overline{p}}\int_V \overline{p'\dot{q}'}\,dV$	11.3	20.0

processes on the temperature and (2) alterations of the flame transfer function, caused by the influence of the temperature distribution on the flow field and reaction rates/flame speed. It is concluded that the change in mode frequency is induced by a significant dependency of the mode frequency on the temperature in the plenum. The results show that neglecting the thermal coupling caused by the heating of the burner yields an incorrect field of speed of sound and consequently an incorrect frequency (Fig. 13).

The performed study illustrates that for LES cases where the adequate prediction of mode frequencies is important, the influence of heat transfer/losses on the results has to be assessed before the computation. Adiabatic boundary conditions may not be sufficient although they can result in mean velocity fields which agree sufficiently well with experiments. As discussed in this paper, simple modeling strategies for heat transfer can already produce more accurate predictions of mode frequencies. However, defining accurate thermal boundary conditions is often a very difficult task, which is also illustrated by the presented results. Therefore, the application of more advanced methods, using coupled simulations that account for both the heat transfer between flow and solid material and inside the solid material, is preferable and will be the focus of future work.

Acknowledgment

The research leading to these results has received funding from the European Research Council under the European Union's Seventh Framework Programme (FP/2007-2013)/ERC Grant Agreement No. ERC-AdG 319067-INTECOCIS.

This work was granted access to the high-performance computing resources of CINES under the allocation x20152b7036 made by Grand Equipement National de Calcul Intensif.

The support of Calmip for access to the computational resources of EOS under allocation P1528 is acknowledged.

The authors would also like to thank the Deutsche Forschungsgemeinschaft, which supported the research leading to the experimental results through the funding of the Collaborative Research Center 606 (SFB 606).

Michael Stoehr is gratefully acknowledged for performing the PIV measurements.

Nomenclature

C_s = Smagorinsky constant
f = frequency
L = air split ratio
l = length scale
p = pressure
P_{th} = thermal power
q = volumetric heat release rate
Q = integral heat release rate
Re = Reynolds number
St = Strouhal number
T = temperature
t = time
V = volume
v = velocity
x = abscissa
y^+ = dimensionless wall distance
γ = isentropic coefficient

Appendix: Additional Material

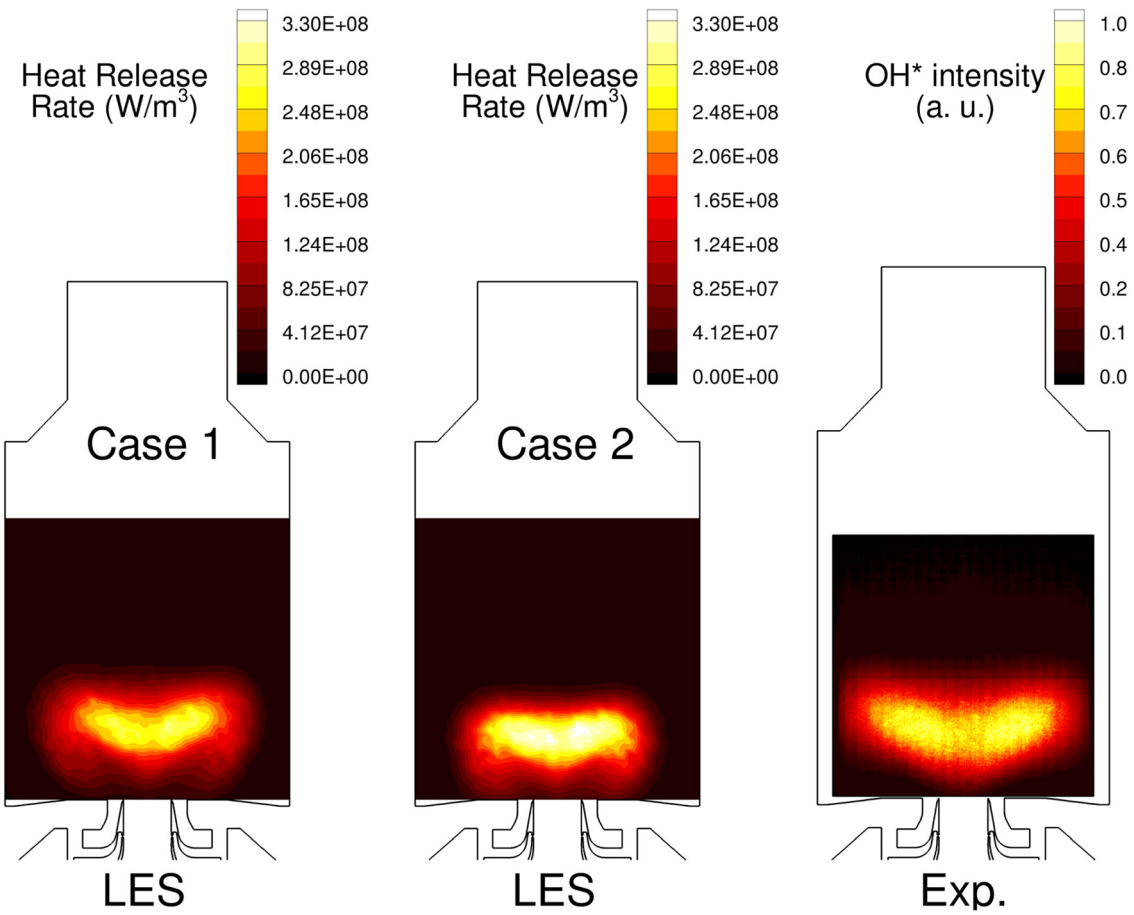

Fig. 13 Average line-of-sight integrated distributions of: the heat release rate in the LESs of cases 1 and 2 and the OH*-chemiluminescence of the flame in the experiment

References

[1] Lieuwen, T., Chang, M., and Amato, A., 2013, "Stationary Gas Turbine Combustion: Technology Needs and Policy Considerations," Combust. Flame, **160**(8), pp. 1311–1314.

[2] Lieuwen, T., 2012, *Unsteady Combustor Physics*, Cambridge University Press, Cambridge, UK.

[3] Hernández, I., Staffelbach, G., Poinsot, T., Román Casado, J. C., and Kok, J. B., 2013, "LES and Acoustic Analysis of Thermo-Acoustic Instabilities in a Partially Premixed Model Combustor," C. R. Méc., **341**(1–2), pp. 121–130.

[4] Roux, S., Lartigue, G., Poinsot, T., Meier, U., and Bérat, C., 2005, "Studies of Mean and Unsteady Flow in a Swirled Combustor Using Experiments, Acoustic Analysis, and Large Eddy Simulations," Combust. Flame, **141**(1–2), pp. 40–54.

[5] Hermeth, S., Staffelbach, G., Gicquel, L., and Poinsot, T., 2013, "LES Evaluation of the Effects of Equivalence Ratio Fluctuations on the Dynamic Flame Response in a Real Gas Turbine Combustion Chamber," Proc. Combust. Inst., **34**(2), pp. 3165–3173.

[6] Ghani, A., Poinsot, T., Gicquel, L., and Staffelbach, G., 2015, "LES of Longitudinal and Transverse Self-Excited Combustion Instabilities in a Bluff-Body Stabilized Turbulent Premixed Flame," Combust. Flame, **162**(11), pp. 4075–4083.

[7] Staffelbach, G., Gicquel, L., Boudier, G., and Poinsot, T., 2009, "Large Eddy Simulation of Self Excited Azimuthal Modes in Annular Combustors," Proc. Combust. Inst., **32**(2), pp. 2909–2916.

[8] Nicoud, F., Benoit, L., Sensiau, C., and Poinsot, T., 2007, "Acoustic Modes in Combustors With Complex Impedances and Multidimensional Active Flames," AIAA J., **45**(2), pp. 426–441.

[9] Emmert, T., Bomberg, S., and Polifke, W., 2013, "Intrinsic Thermoacoustic Instability of Premixed Flames," Combust. Flame, **162**(1), pp. 75–85.

[10] Hoeijmakers, M., Kornilov, V., Lopez Arteaga, I., de Goey, P., and Nijmeijer, H., 2014, "Intrinsic Instability of Flame-Acoustic Coupling," Combust. Flame, **161**(11), pp. 2860–2867.

[11] Courtine, E., Selle, L., and Poinsot, T., 2015, "DNS of Intrinsic ThermoAcoustic Modes in Laminar Premixed Flames," Combust. Flame, **162**(11), pp. 4331–4341.

[12] Duchaine, F., Boudy, F., Durox, D., and Poinsot, T., 2011, "Sensitivity Analysis of Transfer Functions of Laminar Flames," Combust. Flame, **158**(12), pp. 2384–2394.

[13] Lohrmann, M., and Büchner, H., 2005, "Prediction of Stability Limits for Lp and Lpp Gas Turbine Combustors," Combust. Sci. Technol., **177**(12), pp. 2243–2273.

[14] Kaess, R., Polifke, W., Poinsot, T., Noiray, N., Durox, D., Schuller, T., and Candel, S., 2008, "CFD-Based Mapping of the Thermo-Acoustic Stability of a Laminar Premix Burner," Center for Turbulence Research 2008 Summer Program, pp. 289–302.

[15] Mejia, D., Selle, L., Bazile, R., and Poinsot, T., 2014, "Wall-Temperature Effects on Flame Response to Acoustic Oscillations," Proc. Combust. Inst., **35**(3), pp. 3201–3208.

[16] Hong, S., Shanbhogue, S. J., Kedia, K. S., and Ghoniem, A. F., 2013, "Impact of the Flame-Holder Heat-Transfer Characteristics on the Onset of Combustion Instability," Combust. Sci. Technol., **185**(10), pp. 1541–1567.

[17] Yi, T., and Santavicca, D. A., 2010, "Flame Transfer Functions for Liquid-Fueled Swirl-Stabilized Turbulent Lean Direct Fuel Injection Combustion," ASME J. Eng. Gas Turbines Power, **132**(2), p. 021506.

[18] Hassa, C., Heinze, J., and Stursberg, K., 2003, "Investigation of the Response of an Air Blast Atomizer Combustion Chamber Configuration on Forced Modulation of Air Feed at Realistic Operating Conditions," ASME J. Eng. Gas Turbines Power, **125**(4), p. 872.

[19] Shahi, M., Kok, J. B., Roman Casado, J., and Pozarlik, A. K., 2015, "Transient Heat Transfer Between a Turbulent Lean Partially Premixed Flame in Limit Cycle Oscillation and the Walls of a Can Type Combustor," Appl. Therm. Eng., **81**, pp. 128–139.

[20] Kraus, C., and Bockhorn, H., 2013, "Experimental and Numerical Investigation of Combustion Instabilities in Swirl-Stabilized Flames Operated in Partially-Premixed Mode," European Combustion Meeting, pp. P5–26.

[21] Arndt, C. M., Severin, M., Dem, C., Stöhr, M., Steinberg, A. M., and Meier, W., 2015, "Experimental Analysis of Thermo-Acoustic Instabilities in a Generic Gas Turbine Combustor by Phase-Correlated PIV, Chemiluminescence, and Laser Raman Scattering Measurements," Exp. Fluids, **56**(4), pp. 1–23.

[22] Lawson, N. J., and Wu, J., 1999, "Three-Dimensional Particle Image Velocimetry: Experimental Error Analysis of a Digital Angular Stereoscopic System," Meas. Sci. Technol., **8**(12), pp. 1455–1464.

[23] Colin, O., Ducros, F., Veynante, D., and Poinsot, T., 2000, "A Thickened Flame Model for Large Eddy Simulations of Turbulent Premixed Combustion," Phys. Fluids, **12**(2000), pp. 1843–1863.

[24] Legier, J. P., Poinsot, T., and Veynante, D., 2000, "Dynamically Thickened Flame LES Model for Premixed and Non-Premixed Turbulent Combustion," Center for Turbulence Research, Summer Program 2000, Stanford, CA, pp. 157–168.

[25] Martin, C., Benoit, L., Nicoud, F., Poinsot, T., and Sommerer, Y., 2006, "Large-Eddy Simulation and Acoustic Analysis of a Swirled Staged Turbulent Combustor," AIAA J., **44**(4), pp. 741–750.

[26] Boileau, M., Staffelbach, G., Cuenot, B., Poinsot, T., and Berat, C., 2008, "LES of an Ignition Sequence in a Gas Turbine Engine," Combust. Flame, **154**(1–2), pp. 2–22.

[27] Schmitt, P., Poinsot, T., Schuermans, B., and Geigle, K. P., 2007, "Large-Eddy Simulation and Experimental Study of Heat Transfer, Nitric Oxide Emissions and Combustion Instability in a Swirled Turbulent High-Pressure Burner," J. Fluid Mech., **570**, p. 17.

[28] Franzelli, B., Riber, E., Gicquel, L. Y., and Poinsot, T., 2012, "Large Eddy Simulation of Combustion Instabilities in a Lean Partially Premixed Swirled Flame," Combust. Flame, **159**(2), pp. 621–637.

[29] Poinsot, T. J., and Lele, S., 1992, "Boundary Conditions for Direct Simulations of Compressible Viscous Flows," J. Comput. Phys., **101**(1), pp. 104–129.

[30] Selle, L., Nicoud, F., and Poinsot, T., 2004, "Actual Impedance of Nonreflecting Boundary Conditions: Implications for Computation of Resonators," AIAA J., **42**(5), pp. 958–964.

[31] Levine, H., and Schwinger, J., 1948, "On the Radiation of Sound From an Unflanged Circular Pipe," Phys. Rev., **73**(4), pp. 383–406.

[32] Peters, M. C. A. M., Hirschberg, A., Reijnen, A. J., and Wijnands, A. P. J., 1993, "Damping and Reflection Coefficient Measurements for an Open Pipe at Low Mach and Low Helmholtz Numbers," J. Fluid Mech., **256**, p. 499.

[33] Gullaud, E., Mendez, S., Sensiau, C., Nicoud, F., and Poinsot, T., 2009, "Effect of Multiperforated Plates on the Acoustic Modes in Combustors," C. R. Méc., **337**(6–7), pp. 406–414.

[34] Mendez, S., and Eldredge, J., 2009, "Acoustic Modeling of Perforated Plates With Bias Flow for Large-Eddy Simulations," J. Comput. Phys., **228**(13), pp. 4757–4772.

[35] Lee, S. H., Ih, J. G., and Peat, K. S., 2007, "A Model of Acoustic Impedance of Perforated Plates With Bias Flow Considering the Interaction Effect," J. Sound Vib., **303**(3–5), pp. 741–752.

[36] Schmitt, P., 2006, "Simulation aux grandes échelles de la combustion étagée dans les turbines à gaz et son interaction stabilité - polluants – thermique," Ph.D thesis, INP Toulouse, Toulouse, France.

[37] Zhou, R., Balusamy, S., Sweeney, M. S., Barlow, R. S., and Hochgreb, S., 2013, "Flow Field Measurements of a Series of Turbulent Premixed and Stratified Methane/Air Flames," Combust. Flame, **160**(10), pp. 2017–2028.

[38] Poinsot, T., and Veynante, D., 2011, *Theoretical and Numerical Combustion*, 3rd ed., CNRS, France.

[39] Rayleigh, J. W. S., 1878, "The Explanation of Certain Acoustical Phenomena," Nature, **18**(455), pp. 319–321.

[40] Schuller, T., 2003, "Self-Induced Combustion Oscillations of Laminar Premixed Flames Stabilized on Annular Burners," Combust. Flame, **135**(4), pp. 525–537.

[41] Durox, D., Moeck, J. P., Bourgouin, J.-F., Morenton, P., Viallon, M., Schuller, T., and Candel, S., 2013, "Flame Dynamics of a Variable Swirl Number System and Instability Control," Combust. Flame, **160**(9), pp. 1729–1742.

[42] Palies, P., Durox, D., Schuller, T., and Candel, S., 2011, "Nonlinear Combustion Instability Analysis Based on the Flame Describing Function Applied to Turbulent Premixed Swirling Flames," Combust. Flame, **158**(10), pp. 1980–1991.

[43] Durox, D., Schuller, T., Noiray, N., and Candel, S., 2009, "Experimental Analysis of Nonlinear Flame Transfer Functions for Different Flame Geometries," Proc. Combust. Inst., **32**(1), pp. 1391–1398.

[44] Lauer, M., and Sattelmayer, T., 2010, "On the Adequacy of Chemiluminescence as a Measure for Heat Release in Turbulent Flames With Mixture Gradients," ASME J. Eng. Gas Turbines Power, **132**(6), p. 061502.